Integrated optic glass microcantilevers with Bragg grating interrogation

Lewis G. Carpenter, Christopher Holmes, Helen L. Rogers, Peter G. R. Smith and James C. Gates

Optoelectronic Research Centre, University of Southampton, Southampton, SO17 1BJ, UK
** lc906@orc.soton.ac.uk*

Abstract: A new method for creating microcantilevers in glass allows integration of optical waveguides and Bragg gratings. Devices are fabricated by high precision sawing, followed by direct UV writing of waveguides with Bragg gratings and then chemical etching to release the freestanding glass structures. Optical measurement of the Bragg gratings together with piezo-actuation allows the mechanical resonances to be probed. By measuring the mechanical damping coefficient of the cantilever as a function of the gas pressure in a vacuum system the transition from the viscous to the molecular flow regime can be observed.

OCIS codes: (220.4610) Optical fabrication; (060.3735) Fiber Bragg gratings.

References and links

1. A. Llobera, V. J. Cadarso, K. Zinoviev, C. Dominguez, S. Buttgenbach, J. Vila, and J. A. Plaza, "Poly(Dimethylsiloxane) Waveguide Cantilevers for Optomechanical Sensing," IEEE Photon. Technol. Lett. **21**(2), 79–81 (2009).
2. J. Merlein, M. Kahl, A. Zuschlag, A. Sell, A. Halm, J. Boneberg, P. Leiderer, A. Leitenstorfer, and R. Bratschitsch, "Nanomechanical control of an optical antenna," Nat. Photonics **2**(4), 230–233 (2008).
3. C. H. Metzger, and K. Karrai, "Cavity cooling of a microlever," Nature **432**(7020), 1002–1005 (2004).
4. D. Kleckner, and D. Bouwmeester, "Sub-kelvin optical cooling of a micromechanical resonator," Nature **444**(7115), 75–78 (2006).
5. E. Gaura, R. Newman, and M. Kraft, *Smart MEMS and Sensor Systems* (Imperial College Press, 2006), Chap. 2.
6. J. Mora, J. Villatoro, A. Díez, J. L. Cruz, and M. V. Andrés, "Tunable chirp in Bragg gratings written in tapered core fibers," Opt. Commun. **210**(1-2), 51–55 (2002).
7. P. Sun, and R. M. Reano, "Cantilever couplers for intra-chip coupling to silicon photonic integrated circuits," Opt. Express **17**(6), 4565–4574 (2009).
8. G. D. Emmerson, C. B. E. Gawith, S. P. Watts, R. B. Williams, P. G. R. Smith, S. G. McMeekin, J. R. Bonar, and R. I. Laming, "All-UV-written integrated planar Bragg gratings and channel waveguides through single-step direct grating writing," IEE Proc. J. Optoelectron **151**, 119–121 (2004).
9. H. L. Rogers, S. Ambran, C. Holmes, P. G. R. Smith, and J. C. Gates, "In situ loss measurement of direct UV-written waveguides using integrated Bragg gratings," Opt. Lett. **35**(17), 2849–2851 (2010).
10. T. K. Gangopadhyay, "Prospects for Fibre Bragg Gratings and Fabry-Perot Interferometers in fibre-optic vibration sensing," Sens. Actuators A Phys. **113**(1), 20–38 (2004).
11. N. V. Lavrik, M. J. Sepaniak, and P. G. Datskos, "Cantilever transducers as a platform for chemical and biological sensors," Rev. Sci. Instrum. **75**(7), 2229–2253 (2004).
12. C. S. Baldwin, *Springer Handbook Of Experimental Solid Mechanics*, W.N. Sharpe Jr., ed., (Springer, 2008), Chap. 14.
13. L. Grave de Peralta, A. A. Bernussi, H. Temkin, M. M. Borhani, and D. E. Doucette, "Silicon-dioxide waveguides with low birefringence," IEEE J. Quantum Electron. **39**(7), 874–879 (2003).
14. X. Chen, M. C. Davies, C. J. Roberts, S. J. B. Tendler, P. M. Williams, J. Davies, A. C. Dawkes, and J. C. Edwards, "Interpretation of tapping mode atomic force microscopy data using amplitude-phase-distance measurements," Ultramicroscopy **75**(3), 171–181 (1998).
15. G. R. Fowles, and G. L. Cassiday, Analytical Mechanics, (Saunders College, 1993), Chap. 3.
16. H. Kumazaki, S. Inaba, and K. Hane, "Pressure dependence of resonance characteristics of the microcantilever fabricated from optical fiber," Vacuum **47**(6-8), 475–477 (1996).

1. Introduction

Microcantilevers are ubiquitous, ultra sensitive structures used in Atomic Force Microscopy (AFM), pico-molar sensing [1] and as optical antennas [2]. Another promising application of microcantilevers is cooling towards the quantum ground state to explore quantum effects of

superposition and entanglement [3,4]. Most microcantilevers are made in silicon as it naturally lends itself to MEMS fabrication. While silicon has a number of useful attributes including crystallographically controlled etching and ready integration of electronics, it is less ideally suited to optics because of its high refractive index, limited transmission at shorter wavelengths and relatively high losses. In contrast, silica is dominant in optics but is more difficult to pattern and etch, particularly for microscopic planar cantilevers where slow gas phase etch rates make fabrication complex and time consuming. Tapered optical fibers provide another route to fabricate micron scale beams, however these do not allow planar integration [5].

A typical silicon MEMS fabrication route [6] involves growth of thermal oxide silica on a silicon substrate, followed by LPCVD deposition of poly-silicon, photolithography to create an etch mask, etching of the poly-silicon and finally removing away the thermal oxide selectively using hydrofluoric acid to leave a free standing silicon structure. However, such a device does not provide an optical waveguide and many further cleanroom steps would be required to do so [7].

In contrast to the complexity of creating waveguides in silicon MEMS our novel approach reported in this paper allows us to fabricate glass microcantilevers without the use of photolithography and produces cantilevers tens of microns thick which would be prohibitively slow to make using conventional etching techniques. We start with a silica-on-silicon substrate and cut grooves through the silica into the underlying silicon substrate using physical micromachining with a precision dicing saw. Direct UV writing [8] is then used to create optical waveguides containing a series of Bragg gratings. The microcantilevers are then released from the substrate by wet etching using potassium hydroxide (KOH) to remove the underlying silicon, leaving the silica cantilever largely untouched. Neither direct UV writing nor physical micromachining require cleanrooms and both are carried out in a regular laboratory. Furthermore both techniques are CAM (computer aided manufacturing) controlled allowing rapid prototyping of structures, avoiding the need for expensive photolithographic masks and the resulting slow development cycle of conventional MEMS devices.

Our integrated optical glass microcantilevers contain Bragg gratings within them to sense mechanical flexure, an example is shown in Fig. 1. By combining the narrow Bragg response with the Q-factor of the intrinsic mechanical resonance of the cantilever, and by making use of phase-sensitive detection we are able to create a system that is both decoupled from unwanted background noise and yet is very sensitive to the ambient environment of the cantilever, and particularly to the damping coefficients of the flexural modes of the beam.

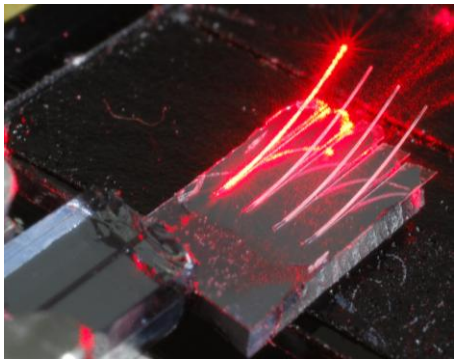

Fig. 1. Glass microcantilever with pigtail couple.

By basing the technology on silica-on-silicon integrated optics, which is widely used in optical telecommunications, and by operating in the 1550 nm window we are able to make use of test and measurement equipment developed for that industry. This brings a further advantage in that the loss of silica is extremely low at these wavelengths, so for example the propagation loss of direct UV written waveguides has recently been shown to be 0.24 $dBcm^{-1}$

[9]. Fiber pigtailing allows us to make robust and low-loss optical connections to our devices with a coupling loss of <0.3 dB per pass. By using the inherent flexibility of direct UV writing we are able to use Bragg gratings at different wavelengths to multiplex signals from several positions on each cantilever through a single optical fiber. This is particularly useful for measurements in vacuum systems by allowing the use of fiber feedthroughs to connect our device to the external laboratory optical measurement system. A further advantage of the use of integrated optical waveguides within the microcantilevers themselves is greater resilience to atmospheric effects such as air currents or changes in moisture. This avoids the need for time intensive alignment, in contrast with the use of free-space optics to measure cantilever position commonly applied in AFM systems [10,11].

2. Structure and fabrication

A number of separate devices with different numbers of cantilevers were fabricated. Figures 2 and 3 show a micrograph image of a typical device with four cantilevers and a close-up of a single cantilever with a length to width aspect ratio of 66:1. In Fig. 2 dotted lines have been added to indicate the path of the optical waveguide which guides light from the input edge of the chip along to the tip of the cantilever.

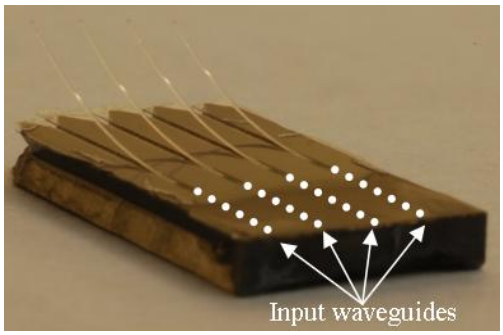

Fig. 2. Microcantilever with waveguides.

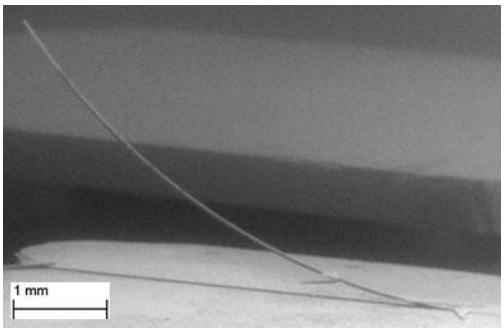

Fig. 3. Microcantilever dimensions.

Bragg gratings are distributed along the whole length of the waveguide allowing strain to be measured both in the cantilever and in the bulk of the chip. The reflection data shown in Fig. 4 is taken from a different device that contained nine cantilevers (not pictured) each being 4 mm in length, 60 μm wide and 50 μm in height. In this case the waveguide contained nine distinct 1mm Bragg gratings equally distributed along 8 μm wide channel waveguides, four located within the substrate and five within the cantilever. The Bragg wavelengths of the sequential gratings along the channel waveguide ranged from 1525 nm to 1565 nm with an equal spectral spacing of 5 nm.

The planar substrates were produced by flame hydrolysis deposition (FHD) and consisted of three layers of refractive index matched silica on a silicon substrate. The middle core silica

layer was doped with boron for index control and with germanium to create photosensitivity for UV writing. The lower cladding was a thick thermal oxide while the overclad was doped with phosphorous and boron to allow index matching to the core and underclad. The first step in the definition of the cantilevers was achieved by physically sawing a cut to define the grooves into the silica layer with a precision dicing saw (Loadpoint MicroAce). This was achieved with 25 μm thick nickel bonded blades running at speeds between 15 and 20 krpm and translation speeds of 0.1-0.5 mms^{-1}. This allowed the length and width of the cantilever to be predefined. To increase the photosensitivity the samples were hydrogen loaded. Waveguides and Bragg reflectors were written into the photosensitive core layer and were aligned carefully relative to the grooves. Finally the device was etched with heated potassium hydroxide (KOH) to free the silica cantilever from the substrate. This was achieved by preferentially etching the silicon from beneath the silica strip defined between adjacent machined grooves. In our experiments a 5 mol concentration of KOH was used; it was heated to 100 °C and was etched for approximately 24 hours. To characterize the microcantilever, the reflection spectra were collected from the microcantilever before and after etching using a broadband source and an optical spectrum analyzer, the spectra are shown in Fig. 4. Note that the final grating at 1565 nm and the input facet were damaged during the wet etching process resulting in the missing spectral peak and ≈10.5 dB of extra coupling loss per pass.

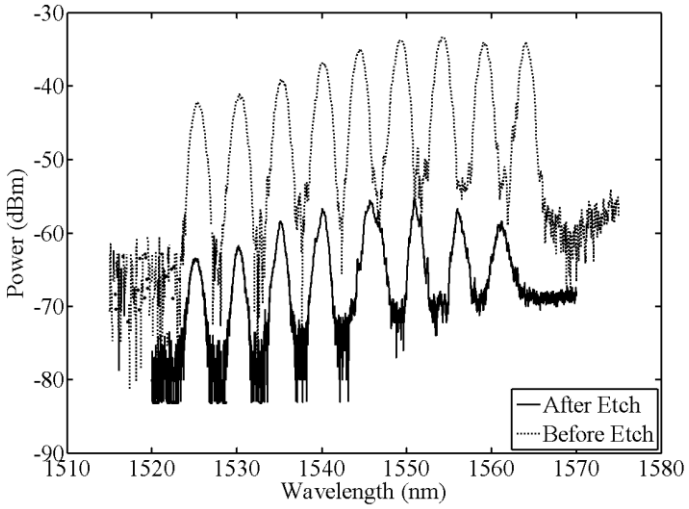

Fig. 4. Bragg grating reflection spectra

3. Theory

The presence of gratings in the waveguides allows us to monitor the local strain at each position along the waveguide. The spectral shift in the Bragg grating's central wavelength is given by the following Eq. (1) [12],

$$\frac{\Delta\lambda_B}{\lambda_B} = \varepsilon - \frac{\varepsilon n_{eff}^2}{2}(p_{12} - \upsilon(p_{11} + p_{12})). \quad (1)$$

where $\Delta\lambda_B$ is the change in central wavelength of the Bragg reflection, λ_B is the central Bragg wavelength, ε is the induced strain, n_{eff} is the effective refractive index for a given wavelength, p_{ij} is the strain-optic tensor and υ is Poisson's ratio. This formula includes both the effect due to length change (grating pitch change) and the strain-optic change of the material's refractive index. The direct UV written waveguide has an $n_{eff} = 1.448$ and assuming FHD silica has similar strain-optic coefficients and Poisson's ratio to PECVD silica the values are as follows $p_{11} = 0.121$, $p_{12} = 0.270$, and $\upsilon = 0.2$ [13]. Thus,

$$\frac{\Delta\lambda_B}{\lambda_B} \approx 0.8\varepsilon. \qquad (2)$$

As Eq. (2) shows the Bragg shift is proportional to strain and dominated by grating elongation, the position of the grating and waveguide within the cantilever must be designed to optimize the response to strain. To increase the strain sensitivity the length must be maximized and the width and thickness must be minimized. Typical dimensions are shown in Fig. 3. The thickness of the silica layers were predefined and yield low-loss single mode optical waveguides at telecom wavelengths.

The glass microcantilever can be used in a similar manner to a tapping mode AFM [14]. The microcantilever is dithered with a piezo to excite a resonant mechanical flexure mode. A narrow laser source is tuned in wavelength to sit on the slope of the Bragg grating peak thus create a signal whose amplitude is proportional to $\Delta\lambda_B$ and consequently the strain in real-time. Phase sensitive detection of the reflected intensity signal at the mechanical oscillation frequency provides a precise measurement of the strain and thus displacement of the microcantilever as well significant suppression of stray noise.

4. Experimental Results

The 6th Bragg grating, with its peak at 1550.9 nm (shown in Fig. 4), was used for the phase sensitive detection as it gave the largest spectral shift, before and after etching, and so its position is clearly sensitive to strain. The Bragg wavelengths of the gratings within the cantilevers shift after etching as a result of stress in the silica layers causing the cantilevers to lift. The tunable laser (Agilent 81689A) was used to match the point of highest gradient of reflection of Bragg grating 6, which was on the grating's shoulder at 1550.7 nm. A piezoelectric transducer was then attached to the substrate and an acoustic signal was sent through the transducer and swept in frequency from 0 to 100 kHz. The reflected optical signal was measured with a photodiode, its signal and the piezo transducer's were sent to a Lock-in Amplifier (SRS830). It was found to be necessary to avoid lower frequencies below 10 kHz due to the presence of relative intensity noise in the laser dominating the signal. An appropriate mechanical resonance was found to be at 29.2 kHz which analysis shows has a Q-factor of 172, shown in Fig. 5. The frequency response showing mechanical resonance of the cantilever and the phase response exhibits the characteristic phase change of a resonance.

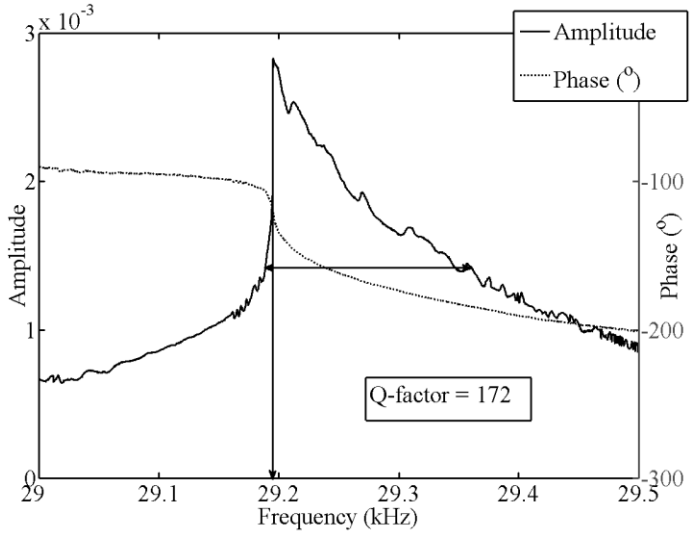

Fig. 5. Cantilever's frequency response

As a test to confirm our mechanical model and our understanding of the microcantilevers we opted to investigate how pressure affects the mechanical resonance response by placing it

in a vacuum chamber. Resonance curves were taken over a pressure range from $1.6\text{x}10^{-2}$ mbar to atmosphere. A damped driven oscillator model Eq. (3) [15] was used to fit the resonance data,

$$A(\omega) = \frac{F_o / m}{[(\omega_o^2 - \omega^2)^2 + 4\gamma^2\omega^2]^{\frac{1}{2}}}. \quad (3)$$

where $A(\omega)$ is the amplitude, F_o is the maximum applied force, m is the mass, ω is the angular frequency, ω_o is the resonant angular frequency and γ is the damping coefficient. The damping coefficient is plotted against pressure for the glass microcantilever's mechanical flexure mode resonance at 29.2 kHz and is shown in Fig. 5. Note that the solid lines are trend lines to guide the eye.

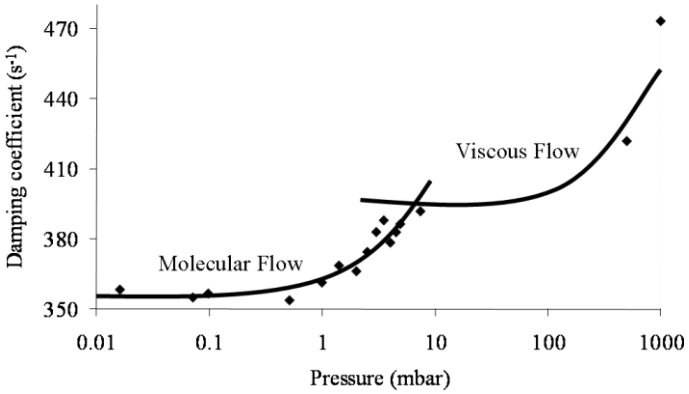

Fig. 6. Calculated damping coefficient

Figure 6 agrees with the trends reported by Kumazaki *et al.* [16] for changes in mechanical resonance of an optical fiber cantilever. The trend lines (to guide the eye) in Fig. 6 exhibit the characteristic transition from molecular flow to viscous flow at around 1mbar. The characteristic increase in damping coefficient is directly related to the decrease in mean free path of the gas particles. Within the molecular flow regime very few gas molecules are present so there are fewer collisions with the cantilever, allowing greater perturbations and *vice versa* for viscous flow.

5. Conclusion

In this letter we have demonstrated a new route to fabricate microcantilevers in glass using direct UV writing and physical micromachining. Both fabrication methods benefit from being CAM based and are implemented outside of the cleanroom. Here these fabrication techniques have been utilized to create a novel glass microcantilever with integrated waveguides and Bragg gratings along its length. The glass microcantilever has been tested within a vacuum system and has shown changes in the damping coefficient due to the transition from molecular to viscous flow. In future we anticipate that silica microcantilevers will be attractive in micro-mechanical quantum ground state experiments due to the lower thermal conductivity and lower optical losses of silica compared to the more conventional silicon.